ChemComm

Accepted Manuscript

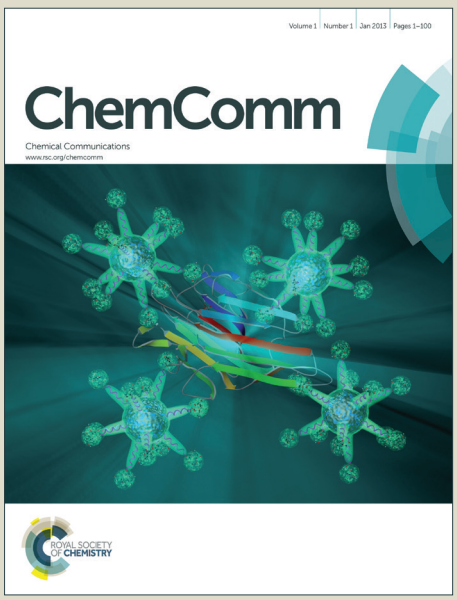

ROYAL SOCIETY OF CHEMISTRY

www.rsc.org/chemcomm

Chem. Commun.

RSCPublishing

COMMUNICATION

Photo-Controlled Targeted Intracellular Delivery of Both Nitric Oxide and Singlet Oxygen Using Fluorescence-Trackable Ruthenium Nitrosyl Functional Nanoplatform

Cite this: DOI: 10.1039/x0xx00000x

Received 00th January 2012,
Accepted 00th January 2012

DOI: 10.1039/x0xx00000x

Hui-Jing Xiang,[†] Lu An,[‡] Wei-Wei Tang,[†] Shi-Ping Yang[‡] and Jin-Gang Liu[†]

A multifunctional nitric oxide (NO) delivery nanoplatform that combines functionalities of target directing, fluorescence tracking, and photo-controlled target attacking was developed. The {Ru-NO@TiO_2 NPs} nanoplatform selectively targeted folate-receptor over-expressed cancer cells while was being simultaneously traced based on its inherent fluorescence. Intracellular localized NO and singlet oxygen were produced on demand by controlled visible light illumination, producing synergistic cytotoxic effect to cancer cells.

Nitric oxide (NO), an endogenously produced biological signaling molecule, plays key roles in various physiological and pathological processes, including vasodilation, immune response, neurotransmission, respiration and apoptosis.[1] The biological functions of this molecule greatly depend on the location, timing, and dosage at which it is released. It is highly imperative to develop a NO-delivery platform that is capable of holding NO stably during storage and subsequently release optimal amounts of NO spatiotemporally at the desired location and time.

Due to its diverse bio-functionalities and promising anticancer activity, NO has stimulated tremendous research interest in the development of NO-releasing molecules as therapeutic agents.[2] Thus far, various classes of exogenous NO-donors have been prepared and applied to biological system for eliciting desired responses, including *S*-nitrosothiols, diazeniumdiolate (NONOates), organic nitrates/nitrites, and metal-nitrosyls.[2-8] Significant efforts have recently been devoted towards the development of light-controlled NO-delivery systems, taking advantage of the noninvasive and highly controllable characteristics of light.[3-8] Some studies have demonstrated the immobilization of metal nitrosyls, such as Ru-NO,[3a] Fe-NO,[4c] and Mn-NO,[5d] onto various matrices, which subsequently release NO upon light illumination. Despite the availability of various NO-donors and NO-delivery platforms, most studies have focused mainly on the feasibility of the system for releasing NO. There is devoid of a definite example for targeted cellular NO delivery, which is essential for minimizing the side effects of NO-mediated therapy.[2]

We report herein a novel NO-delivery nanoplatform which consists of a ruthenium nitrosyl donor, $[Ru(tpy^{COOH})(DAMBO)NO](PF_6)_3$, a target directing molecule of folic acid (FA), and a carrier of biocompatible titanium dioxide nanoparticles (TiO_2 NPs) (Fig. 1). This {Ru-NO@TiO_2 NPs} nanoplatform is capable of delivering NO preferentially to the folate-receptor (FR) overexpressed cancer cells and producing singlet oxygen ($^1O_2$) simultaneously under controlled exposure to visible light. To the best of our knowledge, this is the first example that demonstrates targeted delivery of NO and $^1O_2$ to specific cell lines. Moreover, this nanoplatform is fluorescence self-trackable in cellular environment, rendering its cellular uptake and internalization processes to be tracked.[8]

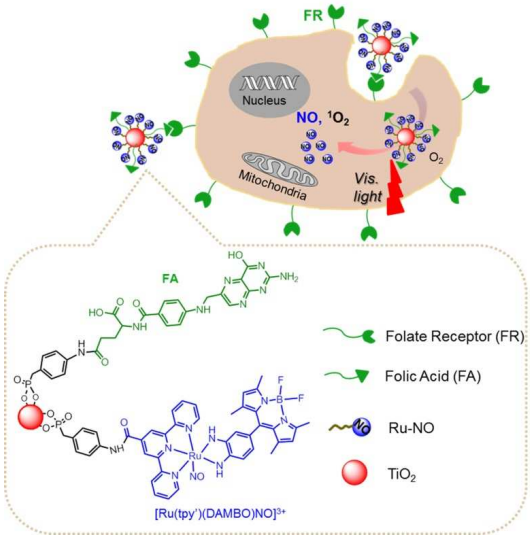

Figure 1 Schematic of the {Ru-NO@TiO_2 NPs} nanoplatform for target-directing delivery of NO and $^1O_2$ to specific cancer cells.

The rationale underlying the construction of this nanoplatform is based on the following concerns: polypyridyl ruthenium nitrosyl was chosen as the NO-donor owing to the low cytotoxicity of ruthenium nitrosyls towards the host cells and their stability against air oxidation, which is desirable for stable NO storage.[3b,5b,5c] Furthermore, ruthenium nitrosyls are photolabile, facilitating NO-delivery upon exposure to light. Targeted NO-delivery is yet another concern that needs to be addressed to minimize the undesirable side effects. FR is a potential marker for carcinomas, which is overexpressed in many of the human cancerous cells. FA has high affinity to FR and thus is a typical cell-targeting agent.[9] FR-derived specificity has been extensively employed in many other drug

delivery systems, while it has never been applied to NO-delivery platform. To this end, FA was chosen as a target-directing molecule in our nanoplatform. Lastly, with regards to the carrier, TiO_2 NPs have widely been used in biomedical applications, such as photodynamic therapy (PDT) and drug delivery, owing to its unique photocatalytic properties, good biocompatibility, and low cytotoxicity.[10] In the given structure, a new ruthenium nitrosyl is employed to sensitize TiO_2 NPs to visible light. Thus, NO and other reactive oxygen species (ROS), such as $^1O_2$, may be simultaneously generated upon illuminating the sensitized TiO_2 NPs with visible light. Taken together, our NO-delivery nanoplatform is designed for specific multimodal anticancer phototherapy.

The preparation of $[Ru^{II}(tpy^{COOH})(DAMBO)NO](PF_6)_3$, **1**, and its functionalized {Ru-NO@TiO_2 NPs} nanoplatform have been depicted in the supporting information. The morphology of {Ru-NO@TiO_2 NPs} as revealed by transmission electron microscope (TEM) indicates an average particle size of 30 nm (Fig. 2A). The diffuse reflectance UV-vis spectrum of {Ru-NO@TiO_2 NPs} showed a prominent broad absorption band at around 548 nm in visible region, suggesting successful sensitization of TiO_2 by the ruthenium nitrosyl (Fig. 2B). The FTIR spectra of {Ru-NO@TiO_2 NPs} demonstrated a ν_{NO} stretching band at 1904 cm^{-1}, which slightly shifted to higher energy relative to that of the uncoupled ruthenium nitrosyl **1** (1912 cm^{-1}, Fig. S4A). The amount of [Ru-NO] incorporated onto the surface of TiO_2 NPs, as analyzed by using energy dispersive spectroscopy, was determined to be 0.81 wt.% Ru. This corresponds to ~0.16 μmol/mg of loaded NO for this nanoplatform. The room temperature photoluminescence (PL) spectra of {Ru-NO@TiO_2 NPs} measured at the excitation wavelength of 400 nm exhibited a typical TiO_2-based PL spectra with three main peaks centered at around 440, 451, and 466 nm (Fig. S4B). This blue fluorescence characteristic makes it possible to track {Ru-NO@TiO_2 NPs} in cells (Fig. S5).

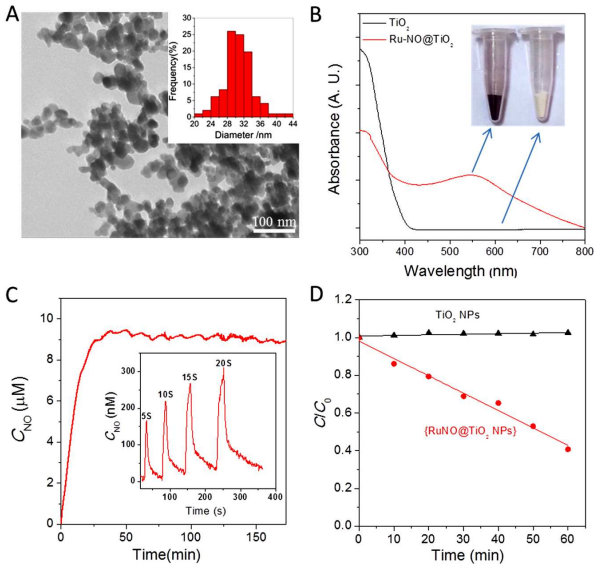

Figure 2 (A) TEM image of {Ru-NO@TiO_2 NPs}. The histogram shown as the inset corresponds to the statistical size distribution of the nanoplatform. (B) Diffuse reflectance UV-vis spectra of {Ru-NO@TiO_2 NPs} (Red line) and TiO_2 NPs (black line). Inset shows the photograph of {Ru-NO@TiO_2 NPs} and TiO_2 NPs. (C) Light-induced NO release from 1.0 mg/mL {Ru-NO@TiO_2 NPs} suspended in anaerobic saline solution by constant light illumination. Inset shows the amperogram of NO-release in response to pulses of light (in seconds). (D) Singlet oxygen species detection by a $^1O_2$ trap CHDDE. Plot of CHDDE relative concentration versus irradiation time catalyzed by {Ru-NO@TiO_2 NPs} (filled circle), and TiO_2 NPs (filled triangle), respectively. Light source: xenon lamp of wavelength λ > 400 nm with longpass filter (300 mW/cm^2).

The feasibility of photo-triggered NO-delivery by the nanoplatform was evaluated in saline solution. Using incremental visible light pulses (5–20 s) illumination of the {Ru-NO@TiO_2 NPs} sample suspended in saline solution resulted in the generation of increased burst of NO (150–300 nM) in solution (Fig. 2C inset). The amount of NO released in this process was typically proportional to the intensity of the applied light (0–300 mW/cm^2) and the duration (0–240 s) of light exposure (Fig. S6A). Under constant illumination of 1.0 mg/mL of {Ru-NO@TiO_2 NPs} in anaerobic saline solution by visible light (300 mW/cm^2), a steady concentration of ~9 μM of NO was observed (Fig. 2C); while in aerobic solution the production of NO was almost terminated after 3.5 h irradiation (Fig. S6B). Furthermore, periodic exposure of light resulted in the generation of periodic burst of NO (Fig. S6C). Accordingly, the photo-induced NO-release properties of this nanoplatform indicate that the dosage of NO delivery can be tuned by control of the exposure to visible light.

Based on the NO concentration measured by a NO-sensitive electrode in aqueous solution, NO quantum yield (Φ) was obtained.[8a, 11] We employed blue (470 nm), green (530 nm) and red (627 nm) light for excitation, and the Φ values of 0.034±0.003, 0.083±0.008 and 0.017±0.002 mol $einsten^{-1}$ were obtained, respectively. The green light (530 nm) excitation produced the largest Φ value among these selected three excitation wavelengths, which is consistent with the nanoplatform electronic absorption in the visible region (Fig. 2B).

Besides being as a NO donor, the ruthenium nitrosyl in the nanoplatform behaves as a photosensitizer as well. Thus, the possibility of producing photogenerated $^1O_2$ species was checked when {Ru-NO@TiO_2 NPs} was irradiated by visible light. Photogenerated $^1O_2$ was monitored by using a trap of sodium 1, 3-cyclohexadiene-1, 4-diethanoate (CHDDE).[12] The photo-generated $^1O_2$ can be measured by UV-vis spectroscopy following the photodegration of CHDDE. Fig. 2D clearly indicates that {Ru-NO@TiO_2 NPs} indeed produced $^1O_2$ upon visible light irradiation. While for the un-sensitized TiO_2 NPs, there was no $^1O_2$ observed under the same experimental conditions as those of {Ru-NO@TiO_2 NPs}. These results together with the above photo-triggered delivery of NO ambiguously demonstrated that the {Ru-NO@TiO_2 NPs} nanoplatform is capable of delivering NO and producing $^1O_2$ at the same time upon visible light irradiation. It is worth commenting that simultaneous producing of NO and $^1O_2$ has important significance for avoiding drug resistance encountered with some conventional drugs through PDT therapies.[2a,8c,12b]

In order to prove the feasibility of FR-mediated targeting, we employed FR-positive [FR(+)] human cervical HeLa cells and FR-negative [FR(-)] human breast MCF-7 tumor cells as a control.[13] Confocal images of the internalized {Ru-NO@TiO_2 NPs} inside the cells were obtained after incubation with the cancer cell lines. Given the photoluminescent properties of {Ru-NO@TiO_2 NPs}, its internalization in cells was readily recognized by its blue fluorescence. Fig. 3A depicts the selective accumulation of {Ru-NO@TiO_2 NPs} in the FR(+) HeLa cells, while its uptake in the FR(-) MCF-7 cells was very less (Fig. 3B). The nanoplatform was found to localize mainly in the cytosol after 30 min of incubation at 37 °C. However, upon extending the incubation period to 8 h, it enters the nuclei of HeLa cells (Fig. S5). According to flow cytometry (FCM) analysis, when the nanoplatform was incubated with the FR (+) HeLa cells, the fluorescence intensity of the cell population increases dramatically (Fig. 3C). Competition experiments, wherein the cells were incubated with free FA (50 μg/mL) and {Ru-NO@TiO_2 NPs} (50 μg/mL), showed a significant

decrease in fluorescence (Fig. 3C). This is indicative of the drastic decrease in cellular surface binding and internalization of {Ru-NO@TiO_2 NPs}. This observation is consistent with the folate-mediated endocytosis of the nanoplatform reported elsewhere.[14] On the other hand, the FR (-) MCF-7 cells showed weak fluorescence above background (Fig. 3D), suggesting its weak cellular association with {Ru-NO@TiO_2 NPs}, and accordingly less cellular uptake of the nanoplatform.

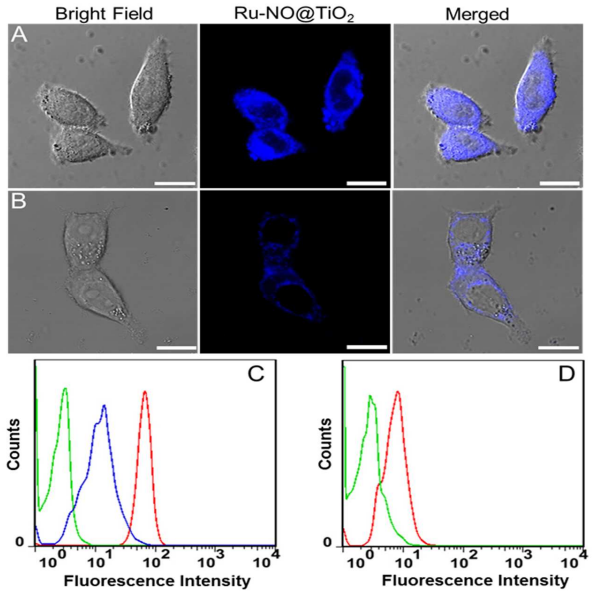

Figure 3 Confocal microscopy images of HeLa (A) and MCF-7 (B) cells treated with 50 μg/mL of {Ru-NO@TiO_2 NPs} for 2 h at 37 °C. The samples were excited at the wavelength of 405 nm and the corresponding fluorescence was recorded in the range of 425–475 nm. Scale bar: 15 μm. (C) Flow cytometry analysis of HeLa cells treated with 50 μg/mL of {Ru-NO@TiO_2 NPs} (red line), 50 μg/mL of {Ru-NO@TiO_2 NPs} + 50 μg/mL of FA (blue line) for 2 h at 37 °C. (D) Flow cytometry analysis of MCF-7 cells treated with 50 μg/mL of {Ru-NO@TiO_2 NPs} for 2 h at 37 °C (red line). The untreated cells were taken as the control (green line).

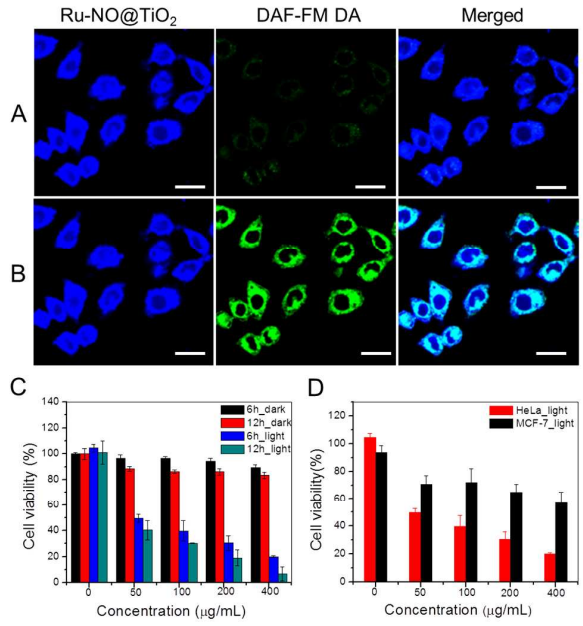

Figure 4 Confocal microscopy images of HeLa cells treated with {Ru-NO@TiO_2 NPs} (50 μg/mL) and DAF-FM DA (5 μM) before (A) and after (B) visible light irradiation (1 min.). The blue and green images were obtained for excitation at 405 and 488 nm, and recording the corresponding fluorescence in the range of 425–475, and 500–550 nm, respectively. (C) Dark and visible light-induced (10 min.) lethality of HeLa cells treated with different concentration of {Ru-NO@TiO_2 NPs} (0 ~ 400 μg/mL) for incubation of 6 h and 12 h, respectively. (D) Mortality of HeLa and MCF-7 cells treated with different concentrations of {Ru-NO@TiO_2 NPs} under visible light illumination (10 min.). Scale bar: 30 μm. Light source: xenon lamp of wavelength λ > 400 nm with longpass filter (200 mW/cm^2).

The intracellular release of NO was confirmed by using a NO-specific fluorescence probe DAF-FM DA.[15] This NO probe is cell membrane permeable and in itself is nonfluorescent. Upon entering into the cells it is hydrolyzed and generates a weakly fluorescent compound, which further reacts with NO to produce a triazole product with strong green fluorescence. The probe was loaded into the cells together with {Ru-NO@TiO_2 NPs}. In the absence of light illumination, only a weak green fluorescence was noticed (Fig. 4A), while a bright green fluorescence was readily observed upon visible light irradiation (Fig. 4B). These experimental results signify the successful *in vitro* intracellular delivery of NO that can be controlled by adept management of visible light.

The formation of cellular ROS after visible light illumination was verified using the ROS probe, DCFH-DA. The probe itself is nonfluorescent and after the oxidation reaction with ROS the oxidized product (DCF) emits a green fluorescence.[16] Confocal microscopy investigation revealed that {Ru-NO@TiO_2 NPs} induced production of ROS in HeLa cells upon visible light irradiation (Fig. S7). FCM analysis also indicated a significant increase in the number of fluorescent cells, and the amount of ROS was proportional to the dosage of applied visible light (Fig. S9).

The cytotoxic effects of {Ru-NO@TiO_2 NPs} towards the FR(+) HeLa and FR(-) MCF-7 cell lines were investigated at various concentrations ranging from 50 to 400 μg/mL using MTT assay. Under dark conditions, the nanoplatform did not exhibit cytotoxic effects for all the concentration ranges tested in this study (Fig. S10). On the other hand, in the presence of visible light irradiation (>400 nm, 200 mW/cm^2, 10 min), the viability of HeLa cells showed a significant decrease (Fig. 4C). The cell survival was inversely related to the concentration of the nanoplatform, as well as with extended incubation periods. The cell death did not result from the illumination of visible light itself, as in the control experiment without nanoplatform the visible light illumination did not lead to cell lethality (concentration = 0, Fig. 4C). Accordingly, it can be concluded that the cell lethality stems from the photo-released/activated active species, such as NO and $^1O_2$, derived from the nanoplatform. In order to differentiate the cytotoxicity effect played by NO and $^1O_2$, a control system {Ru-Cl@ TiO_2 NPs} without coordinated NO was tested for cytotoxicity study, in which the ruthenium coordinated with a chloride. The {Ru-Cl@TiO_2 NPs} showed similar efficiency of generating $^1O_2$ to that of {Ru-NO@TiO_2 NPs} under visible light irradiation (Fig. S9A). Nevertheless, much less photo-cytotoxicity was observed for {Ru-Cl@TiO_2 NPs} when comparing with that of {Ru-NO@TiO_2 NP} under the same experimental conditions. For example, in the dosage of 400 μg/mL nanoplatform for 6 h incubation, ~20% of cell viability was observed for {Ru-NO@TiO_2 NP}, while for {Ru-Cl@TiO_2 NP} the cell viability was remained as high as ~59% after visible light irradiation (Fig. S11B). This results clearly indicates that the cytotoxicity effects are due to both of the released NO and $^1O_2$.

Notably, we found much higher cell viability when the nanoplatform was incubated with the FR(-) MCF-7 cells that were illuminated by visible light under the same conditions of HeLa cells (Fig. 4D). It can be rationalized that the low level of FR at the cell membrane resulted in much less amount of the nanoplatform accumulated in the FR(-) MCF-7 cells. As a result, under the same conditions, the FR(+) HeLa cells uptake more nanoplatform than the

MCF-7 cells, thereby contributing to significantly higher lethality of HeLa cells.

The mechanism associated with the cytotoxicity of {Ru-NO@TiO_2 NPs} was further elucidated by FCM using the Annexin V/PI assay. The intensity of apoptosis fluorescence was found to increase significantly with increase in the concentration of the nanoplatform (Fig. 5). The increasing trend was in accordance with the results observed in cytotoxicity studies. The proportion of live, dead, and apoptotic cells, as determined by FCM, indicated that the cell death caused by the nanoplatform under visible light illumination was mainly through early apoptosis (Fig. S12).

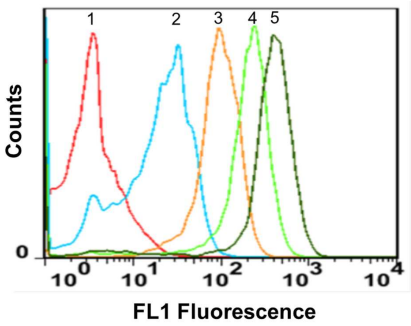

Figure 5 Flow cytometric analysis of FR (+) HeLa cells treated with different concentrations of the {Ru-NO@TiO_2 NPs} nanoplatform (1: 0; 2: 50; 3: 100; 4: 200; 5: 400 μg/mL) under visible light irradiation (> 400 nm, 200 mW/cm^2, 10 min).

The stability of the nanoplatform was finally evaluated (Fig. S13). {Ru-NO@TiO_2 NPs} was stable over a period of half-year when it was kept in solid state at room temperature in the dark. When {Ru-NO@TiO_2 NPs} was stored in saline solution or in cell culture medium in the dark for weeks, there was also no leaching of ruthenium nitrosyl from the carrier, owing to the covalent attachment of ruthenium nitrosyl to the surface of TiO_2 NPs. Furthermore, the nanoplatform also showed good stability even under acidic conditions.

In summary, we have developed a novel multifunctional NO-delivery nanoplatform that is capable of preferentially targeting specific cancer cell lines and subsequently photo-triggered intracellular producing of both NO and $^1O_2$ that to kill cancer cells synergistically. The {Ru-NO@TiO_2 NPs} nanoplatform inherently exhibits blue fluorescence in cellular environment, which makes it suitable for tracing its cellular uptake and internalization processes. The nanoplatform is stable, and is also mended for other target-directing modification, thus offering great potential for precise co-delivery of NO and $^1O_2$ in targeted sub-cellular sites on demand. It could have significant implications for multimodal phototherapy.

This study was financially supported by the NSF of China (21271072), the Program for Professor of Special Appointment (Eastern Scholar) at the Shanghai Institutions of Higher Learning, and sponsored by the Shanghai Pujiang Program (13PJ1401900).

Notes and references

[a] *Key Laboratory for Advanced Materials of MOE & Department of Chemistry, East China University of Science and Technology, Shanghai, 200237, P. R. China, E-mail: liujingang@ecust.edu.cn*

[b] *Key Laboratory of Resource Chemistry of MOE & Shanghai Key Laboratory of Rare Earth Functional Materials, Shanghai Normal University, Shanghai, 200234, P. R. China, E-mail: shipingy@shnu.edu.cn*

† Electronic Supplementary Information (ESI) available: Experimental details and additional figures. See DOI: 10.1039/c000000x/

1 a) L. J. Ignarro, *Nitric oxide biology and pathobiology*, 1st Ed., Academic Press, San Diego, **2000**; b) S. Singh, A. K. Gupta, *Cancer Chemother. Pharmacol.* **2011**, *67*, 1211.

2 a) S. Huerta, S. Chilka, B. Bonavida, *Intl. J. Oncology* 2008, **33**, 909; b) N. Naghavi, A. de Mel, O. S. Alavijeh, B. G. Cousins, A. M. Seifalian, *Small* 2013, **9**, 22; c) A. B. Seabra, N. Duran, *J. Mater. Chem.* 2010, **20**, 1624; d) M. C. Jen, M. C. Serrano, R. van Lith, G. A. Ameer, *Adv. Funct. Mater.* 2012, **22**, 239; e) J. Saraiva, *J. Drug Delivery* 2011, 936438; f) D. A. Riccio, M. H. Schoenfisch, *Chem. Soc. Rev.* 2012, **41**, 3731; g) J. Kim, G. Saravanakumar, H. W. Choi, D. Park, W. J. Kim, *J. Mater. Chem. B* 2014, **2**, 341.

3 a) E. Tfouni, F. G. Doro, A. J. Gomes, R. S. da Silva, G. Metzker, P. G. Z. Benini,D. W. Franco, *Coord. Chem. Rev.* 2010, **254**, 355; b). E. Tfouni, D. R. Truzzi, A. Tavares, A. J. Gomes, L. E. Figueiredo, D. W. Franco, *Nitric Oxide* 2012, **26**, 38.

4 a) P. C. Ford, *Nitric Oxide* 2013, **34**, 56; b) P. C. Ford, *Acc. Chem. Res.*2008, **41**, 190; c) P. T. Burks, J. V. Garcia, R. GonzalezIrias, J. T. Tillman, M. Niu, A. A. Mikhailovsky, J. Zhang, F. Zhang, P. C. Ford, *J. Am. Chem. Soc.*2013, **135**, 18145.

5 a) M. J. Rose, P. K. Mascharak, *Curr. Opin. Chem. Biol.* 2008, **12**, 238; b) M. J. Rose, P. K. Mascharak, *Coord. Chem. Rev.* 2008, **252**, 2093; c) N. L. Fry, P. K. Mascharak, *Acc. Chem. Res.* 2011, **44**, 289; d) B. J. Heilman, J. St. John, S. R. J. Oliver, P. K. Mascharak, *J. Am. Chem. Soc.* 2012, **134**, 11573;

6 a) S. Sortino, *Chem. Soc. Rev.* 2010, **39**, 2903; b) S. Sortino, *J. Mater. Chem.* 2012, **22**, 301.

7 S. Diring, D. O. Wang, C. Kim, M. Kondo, Y. Chen1, S. Kitagawa, K.-i. Kamei, S. Furukawa, *Nat. Commun.* 2013, **4**, 2684.

8 There are already several examples that demonstrated NO photo-releasing while be fluorescent tracked, but targeted NO delivery has not yet been realized. *see* a) M. J. Rose, N. L. Fry, R. R. Marlow, L. Hinck, P. K. Mascharak, *J. Am. Chem. Soc.* 2008, **130**, 8834; b) N. L. Fry, J. Wei, P. K. Mascharak, *Inorg. Chem.* 2011, **50**, 9045; c) A. Fraix, N. Kandoth, I. Manet, V. Cardile, A. C. E. Graziano, R. Gref, S. Sortino, *Chem. Commun.* 2013, **49**, 4459.

9 a) J. Sudimack, R. J. Lee, *Adv. Drug Deliv Rev.* 2000, **41**, 147; b) P. S. Low, W. A. Henne, D. D. Doorneweerd, *Acc. Chem. Res.* 2008, **41**, 120.

10 Z. F. Yin, L. Wu, H. G. Yang, Y. H. Su, *Phys. Chem. Chem. Phys.* 2013, **15**, 4844.

11 M. G. Sauaia, R. G. de Lima, A. C. Tedesco, R. S. da Silva, *J. Am. Chem. Soc.* **2003**, *125*, 14718.

12 a) V. Nardello; D. Brault; P. Chavalle; J. M. Aubry, *J. Photochem. Photobiol. B* 1997, **39**, 146; b) C. Ratanatawanate; A. Chyao; Jr. K. J. Balkus, *J. Am. Chem. Soc.* 2011, **133**, 3492.

13 H. Chen, R. Ahn, J. V. den Bossche, D. H. Thompson, T. V. O'Halloran, *Mol. Cancer Ther.* 2009, **8**, 1955.

14 a) J. Sudimack, R. J. Lee, *Adv Drug Deliv Rev.* 2000, **41**, 147; b) Y. Lu, P. S. Low, *Adv. Drug Deliv. Rev.* 2002, **54**, 675.

15 H. Kojima, Y. Urano, K. Kikuchi, T. Higuchi, Y. Hirata, T. Nagano *Angew. Chem. Int. Ed.* 1999, **38**, 3209.

16 J. Tian; L. Ding; H.-J. Xu; Z. Shen; H. Ju; L. Jia; L. Bao; J.-S. Yu, *J. Am. Chem. Soc.* 2013, **135**, 18850.

